Hybrid QM/MM and classical molecular dynamics simulation of Amadori product in γB-crystallin

Alaa El-Din A. Gawad

Biophysics and Laser Science Unit, Research Institute of Ophthalmology, Giza, Egypt
alaael_din3@hotmail.com

Abstract: Glycation process compromises proteins throughout the body, thus is a key feature of diabetes-related complications. Classical and combined QM/MM molecular dynamics (MD) simulations have been performed to study the glycation effect D-β-fructopyranose on γB-crystallin. Molecular details associated with formation a Schiff base were investigated in terms of electrostatic potential, RMSD, RMSF, radius of gyration, secondary structure alterations, radial distribution functions, and disruption of ion pair network. The results of the QM/MM MD simulations have been found in good agreement with experimental values, proving that backbone stability and protein size have not been changed. However, the formation of Schiff base leads to alterations of tertiary structure of γB-crystallin and disturbance of ion pair network.
[Alaa El-Din A. Gawad. **Hybrid QM/MM and classical molecular dynamics simulation of Amadori product in γB-crystallin.** *Life Sci J* 2013; 10(4): 1923-1932]. (ISSN: 1097-8135). http://www.lifesciencesite.com. 255

Keywords: MD simulations, QM/MM, Millard reaction, protein stability, γB- crystallin.

1.Introduction

Non-enzymatic glycation play an important role in diseases. It has a huge impact on the physical and functional properties of proteins (*Karve and Cheema, 2011*; Yang *et al.*, 2013). Glycation process originates from the interaction between -amino group and sugar (Millard reaction) giving rise to an unstable Schiff base adducts to form fructosylysine; then degrading to a variety of carbonyl compounds that are much more reactive than the original sugar molecule (*Baynes et al., 1989*). Moreover, Amadori products proceed very slowly to form many different adducts and crosslinks – some of which are fluorescent and coloured ‘‘browning pigments’’ (*Yin and Chen, 2005; Neves, 2013*).

Glycation of lens crystallins is considered to be a causative factor in age-related and diabetic cataracts (*Swamy and Abraham, 1987*). The rate of glycation process is enhanced in the diabetic lens compared to senile lens proteins (*Duhaiman, 1995*). Nonetheless, the level of lens sugar alone is not the only determining factor of lens protein glycation (*Jansirani and Anathanaryanan, 2004*). Thus the reduced sugars increased cross-linking of lens crystallins that may cause aggregation followed by precipitation of lens proteins (*Hollenbach et al., 2003; Michael and Bron, 2011*). β-D-fructopyranose is the preponderant tautomer and it accounts for 69.6% in water at room temperature (Mega *et al.*, 1990). Under conditions of severe hyperglycaemia, high fructose intake promotes the development of cataracts in the lens of the eye (Bell *et al.*, 2000; Gul *et al.*, 2009).

Among the three calf lens structural proteins, the monomeric γ-crystallins comprised about 20% and exist in larger amounts in the nucleus than in the cortex (*Sharma and Santhoshkumar , 2009*). γB-crystallin is the most abundant γ-crystallin fraction and is remarkably stable (*Mandal et al., 1987*). It has been demonstrated that Lys-2 residue accounts for about 50% of the total glycation by all the sites (*Casey et al., 1995*). However, docking studies revealed γ-crystallins have non-covalent multiple different glucose binding sites (*Alaa, 2012*).

There is a growing body of evidence that computer simulations are important tools to tackle many of the complex problems, e.g. nanotechnology and the need to understand physical phenomenon, because of the lack of experimental techniques or working models (*Salim and Zaidi, 2003; Xia et al., 2013; Alaa and Medhat, 2013*). Moreover, recent development of hybrid theoretical approaches made it possible to divide large molecular systems into several subsystems (layers) and to treat them at different levels (*Lin and Truhlar, 2007; Lodola et al., 2008*). Both classical and QM/MM molecular dynamics simulations have been used extensively to model the enzymatic reaction mechanisms, the interaction energy of protein-ligand complex, differences in reactivity between several derivatives, and predicting their spectroscopic and exited state properties (*Steinbrecher and Elstner, 2013*). However, the accuracy of the calculation depends strongly on description of the QM subsystem at the molecular orbital (MO) theoretical level and the size of the QM region (*Mulholland, 2007).*

$$H_{total} = H_{QM} + H_{MM} + H_{QM/MM}$$

Where H_{QM} and H_{MM} are the hamiltonians for the quantum mechanical (QM) and classical (MM for molecular mechanical) regions, respectively, calculated in a standard way. $H_{QM/MM}$ describes the

interaction between the QM and MM regions, and can be treated in various ways.

Here, a comprehensive theoretical study on Schiff base of γB-crystallin by using molecular mechanics as well as with a simulation using a QM/MM implementation with the Self Consistent Charge Density-Functional Tight-Binding (SCC-DFTB) method (*Elstner et al., 1998*) with the well-established AMBER force field, which has been successfully applied in the fields of extended systems, including enzymes (*Wickstrom et al., 2009*). But to the best of our knowledge, it has not been applied in the studies of the Schiff base of lens crystallins. Therefore, considering the lack of structural data of the early stage of glycated lens crystallins and a full atomistic description is urgently needed for the future optimization for geometrical and/or electronic properties of these structures. In this methodology, it was also planned to compare the results with published biophysical data.

2. Materials & Methods:

1. Preparation of complex

In the simulations that mimicked the state in which the Schiff base formed, a molecular model was constructed using the refined x-ray crystal structure of the bovine γB-crystallin (Protein Data Bank code 1AMM). This experimental protein structure coordinates have been chosen because it has a relatively high experimental resolution (1.2 Å) (*Kumaraswamy et al., 1996*). In the crystal, there are two almost identical monomers in the asymmetric unit, so one monomer is chosen as the computational model. The protonation state of each ionizable side chain of histidine residue in γB-crystallin was changed into protonated ε-nitrogen (*Garner and Balaji, 1988*). A model for fructopyranose was built using PRODRG (*Schüttelkopf and van Aalten, 2004*). The atomic partial charges of fructopyranose were derived with the R.E.D.-IV program (*Vanquelef et al., 2011*), using the rigid body reorientation algorithm and the RESP-C2 model for the charge fitting. The quantum mechanics software used was Gaussian_2009_C.01 (*Gleeson et al., 2003*) at the Hartee-Fock level with the HF/6-31G*//HF/6-31G*-CHELPG algorithm used in molecular electrostatic potential (MEP) computation. The carbohydrate moiety at carbon C-1 connected to Lys-2 of γB-crystallin.

2. Classical Molecular Mechanics:

The Xleap module of AMBER was used for preparing the input files. All simulations were performed according to the standard protocols, which consists of energy minimization, followed by gradual heating of the system. All simulations were performed using the AMBER12 software package (*Salomon-Ferrer et al., 2013*). Topology and parameter files for the protein were generated using ‘‘ff99SB’’ force field (*Hornak et al., 2006*).

The obtained complex of fructopyranose-γB-crystallin was soaked in 8440 of a periodic cuboidal box of TIP3P water molecules (*Mark and Nilsson, 2001*). One atom of Na^+ was added to the system to adjust the charge to neutral. Then in the first minimization run, the complex was minimized using 1500 steps of steepest descent and 1000 steps of conjugate gradient method as the protein and ligand atoms were fixed with a force constant of 500 Kcal mol^{-1} $Å^{-2}$, and water residues were allowed to move. Then the whole system was minimized using 5000 steps of conjugate gradient. A cut-off of 10 Å was used. After minimization, the system was heated slowly to 300 K at constant volume (NVT) over a period of 15 picoseconds, using harmonic restraints of 10 $Kcal^{-1}mol^{-1}A^{-2}$ on the solute atoms. The integration time-step was 2 fs. Then the system was allowed to equilibrate for 15 ps using a *Langevin* thermostat (*Pastor et al., 1988*) to maintain the temperature of the system at 300 K. SHAKE constraints (*Ryckaert et al., 1977*) were applied to all hydrogen bonds. In order to maintain the pressure, we used isotropic position scaling with a relaxation time of 2 ps.

The production simulation of complex was performed under NPT conditions where the temperature was kept at 300 K and the pressure at 1 atm to remain consistent with experimental conditions. All simulations were performed with the weak coupling algorithm (*Berendsen et al., 1984*) to control the temperature of the simulation box during simulation.

3. QM/MM Simulations

The initial γB-crystallin-fructose model prepared as described above was partitioned into a QM subsystem and a MM subsystem. The QM subsystem (61 atoms) comprises Lys 2, Arg 36, Asp 38, fructose and three waters. The standard SCC-DFTB is used for the QM region. The SCC-DFTB approach is chosen based on its overall balance of computational efficiency and accuracy. For the MM subsystem, all other residues and the surrounding water molecules are described by the AMBER ff99SB force field. The boundary between the QM and MM subsystems was treated using the link atom approach (*Lin and Truhlar, 2005*). Then, the system was solvated with 28688 water molecules that formed a water TIP3P cubic box of 25 Å. A periodic boundary condition (PBC) is employed for the water box. Finally, a number of 2 Na^+ ions were used to neutralize the system at random positions. The system is then subjected to two consecutive minimization steps. In first step, water molecules and

ions are allowed to move freely for a 1000 steps of steepest descent minimization. During minimization, protein and ligand atoms are constrained to their original positions by a force constant of 500 kcal·mol^{-1} Å^{-2}, followed by 1500 steps of conjugate gradient minimization for the whole system with no constraints. Following minimization, two consecutive steps of heating and equilibration are performed. First; the system is gradually heated in the NVT ensemble from 0°K to 300°K for 30 ps with a time step of 1 fs, applying a force constant of 500 kcal·mol^{-1} Å^{-2} on the protein and ligand coordinates, and using *Langevin* dynamics with the collision frequency γ of 2 ps^{-1} for temperature control. A further 100 ps simulation in the NPT ensemble is performed to equilibrate the system density applying a time step of 0.5 fs, which requires the use of SHAKE algorithm (*Ryckaert et al., 1977*) to constrain all bonds involving hydrogen atoms. The temperature is controlled using Berendsen temperature control and is kept at 300°K. The pressure is kept at 1 atm applying a Berendsen barostate with a pressure relaxation time of 1ps. In all simulation steps, long-range electrostatics is computed using the particle mesh Ewald (PME) (*Darden et al., 1993*) with a non-bonded cut-off of 8 Å. The edge effect is removed by applying periodic boundary conditions. All MD simulations are carried out using the sander module of AMBER12. Finally, a production 20 ps long MD simulation was performed. Each window of the simulation was sampled with 0.5 ps of equilibration and production dynamics.

The proportions and the complex electronic structure of the molecule studied make the quantum-chemical calculations quite demanding. Because of the SCC-DFTB procedure converge slowly, leading to prolonged computational time, electronic temperature flag in AMBER suite used to accelerate SCC convergence in DFTB calculations.

The resulting trajectories were analyzed by PTRAJ module of AMBER package and VMD (*Humphrey et al., 1996*).

3. Results:

Prior to investigate the effect of Millard reaction of γB-crystallin through computational method, it is of vital importance to obtain an accurate model of the protein-ligand complex. The binding of a fructose to γB-crystallin was used as a representative model of Amadori product. Molecular dynamics simulations were performed to elucidate the molecular events of binding a fructose molecule to Lys-2 residue in γB-crystallin in explicit solvent. The analysis of the potential energy for native and glycated γB-crystallin trajectories (5 ns) showed that both systems were stable over the course of the simulation (*Figure 1)*. Both simulations have converged to a constant average potential energy over the nanosecond time scale significantly, the solute did not directly interact with its periodic image.

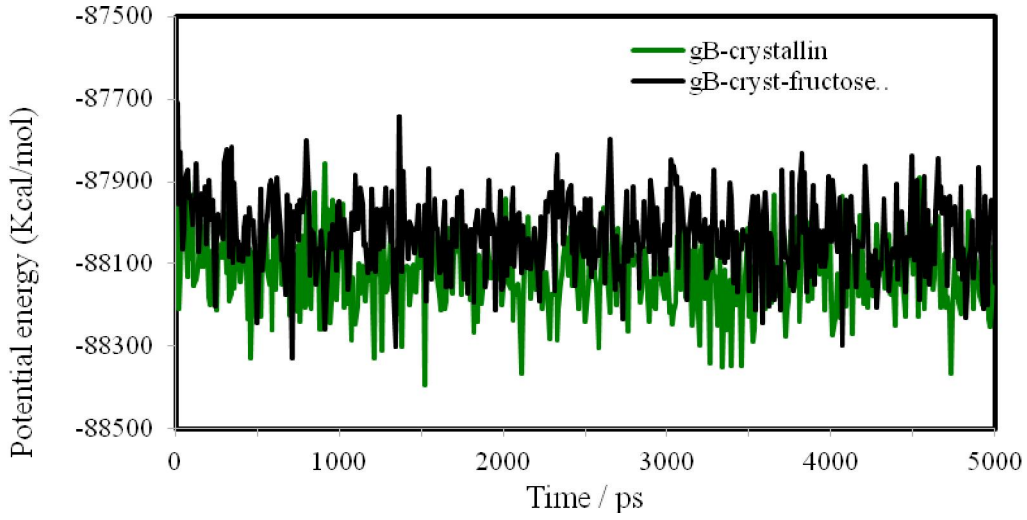

Figure (1): Potential energy plot of MD simulation for glycated and native γB-crystallin.

The RMSD profiles are also useful approach for assessing the stability of an MD simulation. This gives an impression of the overall structural differences between the initial model structure and each of the structures extracted sequentially from the trajectory. The RMSD between the first coordinate and the generated structures in the trajectory was depicted in Figure (2). Therefore RMSD values for the main chain atoms (N, Cα, C) of native and glycated γB-crystallins during 5ns simulation time were calculated. As revealed in figure (2) simulation of the two structures during this time period showed

good stability. This Structural stability is demonstrated by the low-protein backbone root mean square deviation (RMSD) of ~1 Å over the whole trajectories.

γB-crystallin is a two-domain protein. The root mean square fluctuations (RMSF) of γB-crystallin were computed to understand how ligand binding might affect protein fluctuation (Figure 3). The RMSF of the native γB-crystallin protein showed two modes of motion; The RMSF of the N-terminal domain is lower than that of the C-terminal domain. On the otherhand, the RMSF after fructose binding suggests that this event significantly dampens protein fluctuation. The baseline for glycated structure fluctuations is shifted higher relative to native protein. However the amplitude of fluctuation for C-terminal domain is higher.

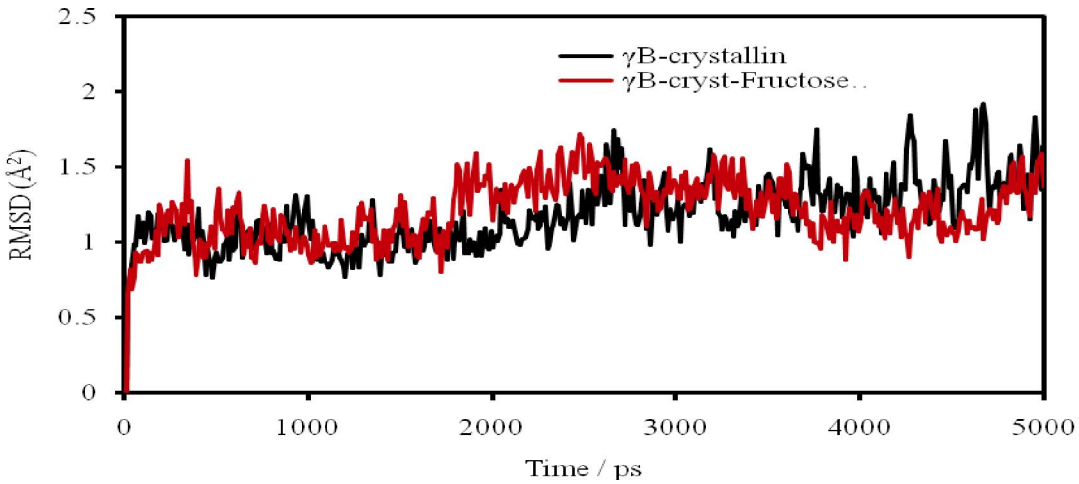

Figure (2): Root mean square displacement of backbone of the glycated and native γB-crystallin as a function of simulation time.

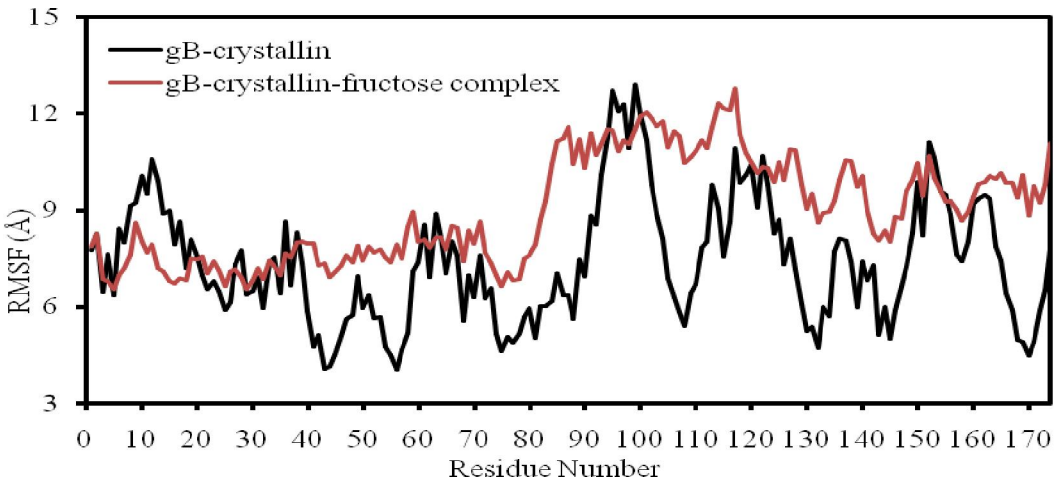

Figure (3): Average residue fluctuations during the entire molecular dynamics simulation

The radius of gyration is a function of the root mean square distance of the atoms from their common centre of gravity, and is therefore related to the size and shape of the molecule. The native and glycated γB-crystallin models showed similar 17-Å^2 of value after 5-ns of MD simulation time. For glycated γB-crystallin, the radius of gyration has similar oscillations upon fructose binding as the

native protein during the whole simulation figure (4). It indicates glycated γB-crystallin keeps the same basic structure along the whole trajectory. Therefore, global conformation or size of the γB-crystallin protein was not heavily changed by the glycosylation during MD simulations.

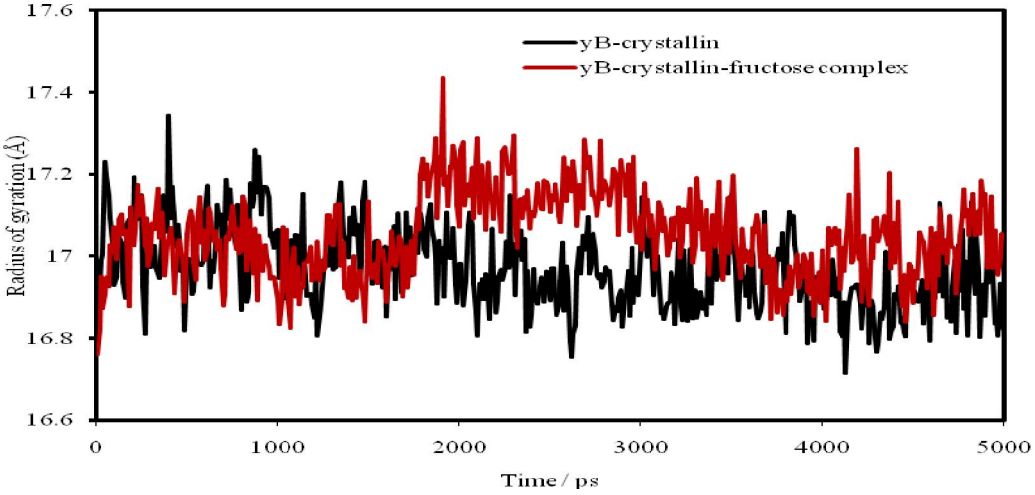

Figure (4): The radius of gyration (RoG) values as a function of time of simulation for both glycated and native γB-crystallin.

Figure (5) shows the secondary structure content throughout each trajectory of γB-crystallin during 5ns MD simulations. The results in figure 5 show that the secondary structures keep stable during 5 ns for γB-crystallin with or without ligand bound, i.e. fructose. Only minor changes in the α-helix were observed.

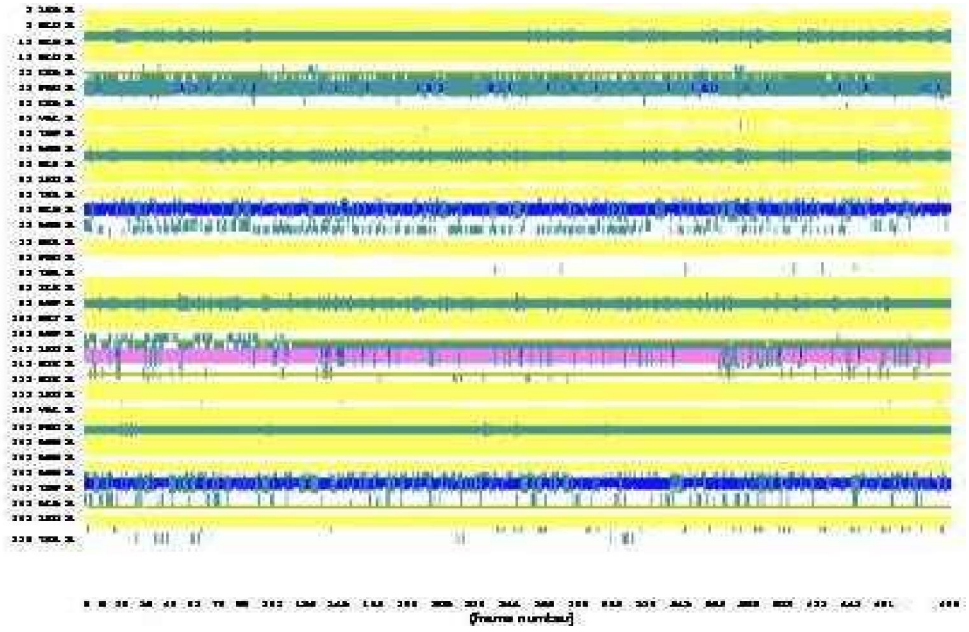

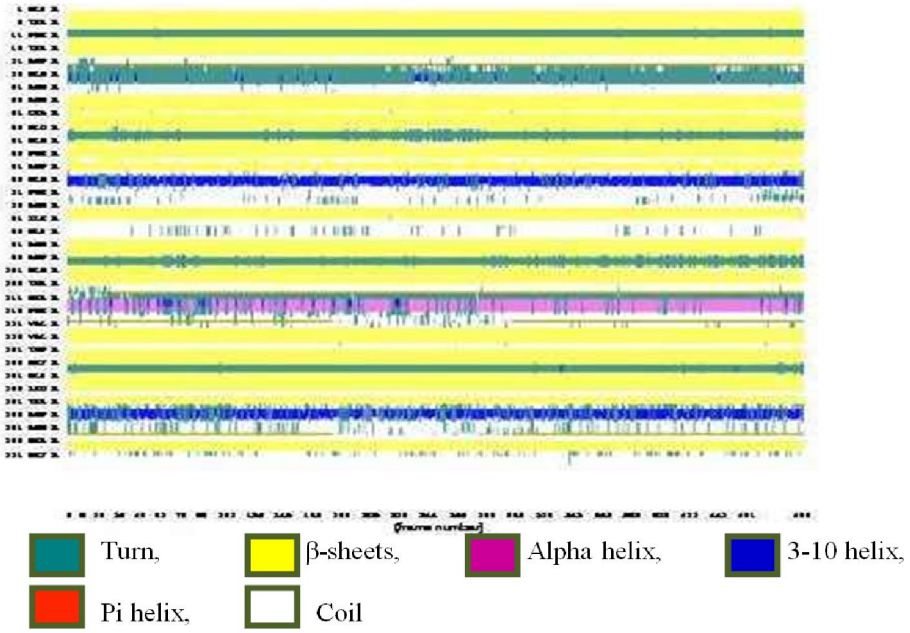

Figure (5)*:* Secondary structure timeline analysis as computed by the timeline plugin contained in VMD**.**

The atoms of full system are partitioned into two layers by imposing a frontier, between the QM and MM layers, at the C1-NZ bond of the Lys-2 side chain. The quantum mechanical (QM) layer includes 21 atoms of the fructosyl moiety, 20 atom of Lys-2, the side chains of GLU17 and ASP38 and 4 hydrogen atoms as link atoms that saturate the extra valence of the terminal -NZ at the boundary. While a QM layer that includes only the Schiff base is sufficient to describe the optimum geometry of the system as well as conformational changes due to rearrangement. To assess systematically the change in the fructosyl geometry that accompanies rearrangement of the Schiff base, we fully optimized the fructosylysine in the aqueous phase using the SCC-DFTB (*Elstner, 2006*) to describe the fructose pucker. It has been shown that relative to full DFT, the SCC-DFTB method the best semi-empirical description of five- and six- membered carbohydrate ring deformation in the gas phase but also in the protein environment (*Barnett and Naidoo, 2010*).

A close examination of the structures of glycated protein reveals certain features for both fructosyl moiety and protein residues. Table (1) shows the computed bond lengths of the fructopyranose ring for minimized and SCC-DFTB/MM level of theory. The bond length of C6-O6 decreases by 0.132 Å while O6-C2 distance increases by 3.592 Å. Then the ring conformation was assessed by monitoring the dihedral angles.

At the Schiff base, the nitrogen atom catalyses a nucleophilic substitution that proceeds via a transient oxocarbenium-like transition state (fructopyranosyl oxocarbenium ion), with an sp^2-hybridised geometry at both C2 (anomeric carbon atom) and O6, allowing a considerable mutual double bond character and resulting in C5–O5–C1–C2 coplanarity. Because the oxocarbenium ion has double-bond character between the anomeric carbon and the ring oxygen, this part of the structure must be planar (Figure 6). This often leads to the formation of cyclic and open forms mixtures but also inevitably to degradation (*Mota et al., 1994*). The nature of ring distortion within the environment of the protein can be characterized by the Cremer-Pople puckering parameters (*Cremer and Pople, 1975*). After 20 ps production phase, puckering parameters of the fructopyranosyl ring was θ= 135.804, φ= 344.928, and Q= 0.663, indicating a shift from chair conformation to half boat.

To calculate the contribution of the Schiff base formation on γB-crystallin, the conformational change for some residues involved in the formation of ion pairs and disulfide bridge were evaluated upon QM/MM simulation. Table 2 summarizes the average distances of some residues involved in the formation of ion pairs and disulfide bridges. The average distance between Lys2-NZ and the carbon C1 of fructopyranosyl ring in the optimized structure was 1.494 Å compared to 1.495 Å upon 20 ps QM/MM simulation. Furthermore, the bond length between Fru-O3 and OE1 and OE2 of Glu17 of optimized structure increases after production phase of QM/MM simulation by 1.944 Å and 2.163Å respectively. Ion

pairs play important roles in protein structure and function of lens proteins. The distances between the carboxylate oxygen atoms (OE1 and OE2) of Glu17 and the Lys2 nitrogen become significantly shorter at the production phase than the optimized counterpart, with values of 4.003 and 4.465 Å and 4.003 and 4.465 Å respectively. The fructopyranosyl adduct formation do not favor the interaction of Cys18 and both of Cys22 and Cys78 in both optimized structure and the SCC-DFTB/MM simulation.

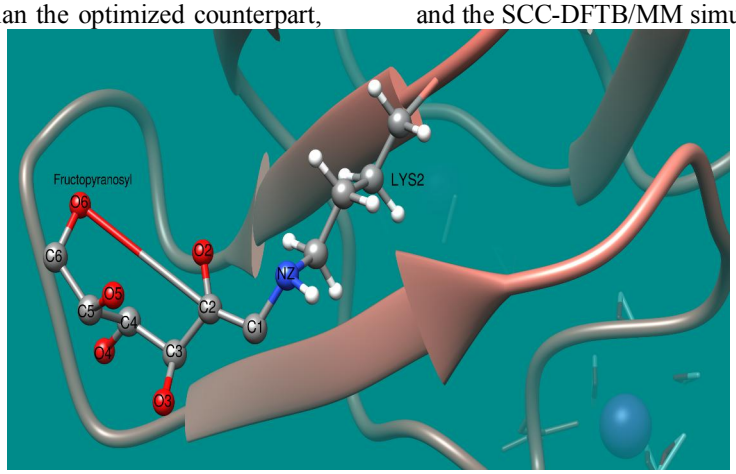

Figure 6: The three-dimensional structure of the glycated γB-crystallin intermediate showing half chair transition conformation.

Table (1). Comparison between bond lengths in angstroms for minimized structure and SCC-DFTB/MM level of theory.

Bond distances of pyranose ring	Optimized structure	SCC-DFTB/MM simulation
C1-C2	1.521	1.486
C2-O2	1.407	1.275
C2-O6	1.436	5.028
C2-C3	1.543	1.540
C3-O3	1.435	1.432
C3-C4	1.539	1.577
C4- O4	1.415	1.435
C4-C5	1.558	1.565
C5-O5	1.422	1.483
C5-C6	1.537	1.548
C6-O6	1.428	1.483

Table 2: Comparison between bond lengths of γB-crystallin in angstroms for minimized structure and SCC-DFTB/MM level of theory[9]

Bond length	Optimized structure	SCC-DFTB/MM simulation
C1….Lys2-NZ	1.494	1.495
Glu17-OE1….Fru-HO3	2.533	4.477
Glu17-OE2….Fru-HO3	3.263	5.426
Lys2-NZ….Glu17 OE1	4.559	4.003
Lys2-NZ….Glu17 OE2	5.486	4.465
CYS18-SG….CYS78-SG	4.046	3.895
CYS18-SG….CYS22-SG	5.308	4.765

Investigations of radial distribution functions, $g(r)$, about different solute atoms can provide insights into changes in local solvent structure due to differences in the overall QM/MM interaction potential. In this study, we calculated radial distribution functions of TIP3P water molecules about the fructosyl moiety and lysine residue of the model. For the distribution of water molecules about the nucleophilic nitrogen, the first solvation shell for glycated and native γB-crystallins are about 2.95Å and 2.85 Å respectively and the peak height for glycated γ-crystallin is twice lower than that for non-glycaed γ-crystallin.

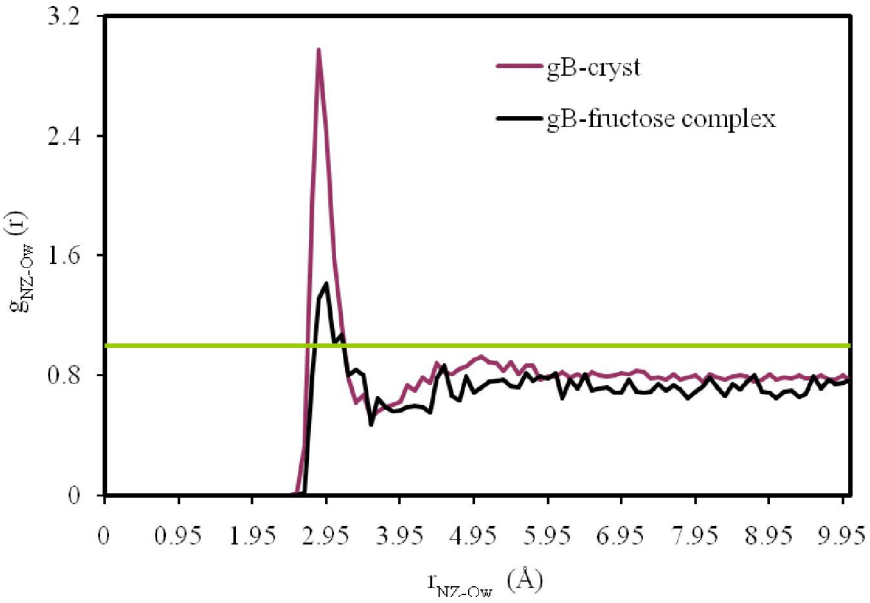

Figure (7): Computed radial distributions functions for native and glycated γB-crystallin structures

4.Discussion

The link between excessive intake of fructose and metabolic syndrome is becoming increasingly established (*Gul et al., 2009*; *Johnson et al., 2010*). Moreover, the refractive index gradient of proteins in the eye lens in the absence of significant solvation effects and ligand binding is generally essential to maintain optical properties of the eye. However, lens crystallins become more susceptible to glycation in diabetes, which play an important role in their etiology (*Franke et al., 2003*).

The overall stability of the glycated γB-crystallin was measured by estimating the potential energy, the root mean square deviation (RMSD) of the molecule, the radius of gyration and secondary structure analysis (Figs 1, 2, 4 and 5). A comparison of the native and glycated protein backbones observed in the present simulations (5 ns) clearly show that adding a cyclic fructose molecule has no marked effect. Liang and Chakrabarti (*1981*) studied the effect of glycosylation with glucose 6-phosphate on the conformation of purified bovine lens proteins. Using circular dichroism (CD) they could demonstrate changes in the near-ultraviolet (UV) CD characteristic of aromatic amino acid residues. However, no changes in the far-UV CD were observed. These results indicate that glycosylation causes a change in tertiary structure of the molecule but that the secondary structure (peptide backbone) is unaffected (*Liang and Chakrabarti, 1981; Beswick and Harding, 1987*).

On the other hand, decrease the fluctuation of the protein residues upon frucopyranose ring binding reflecting rearrangements in response to environmental changes (Fig. 3). In other words, the relative mobility of different regions of the protein is deteriorated. These correspond with the change of distances between hydrophobic areas of contact between the two domains in the γB-crystallin concluding that the side-chain and backbone motions in these areas are dampened. This is the case for Met43, Phe56, Ile18 residues (N-terminal) which are in the proximity of Val132, Leu145, and Val170 residues of the opposite domain (C-terminal) (unpublished data). It has been reported that glycosylation of a folded protein does not affect the torsion angles of the backbone, whereas a dampening effect of glycans on backbone fluctuation in both the native and the unfolded states of peroxidase were obtained (*Imperiali and O'Connor, 1999; Tams and Welinder, 2001*).

Previous studies showed the interaction of sugars with Nε-lysine of γB-crystallin is responsible for cross-linking ability of the protein, which depends not only upon the level of glycation but also upon which amino group is glycated (*Zhao et al., 1997*). The binding of cyclic fructose affect the protonation state of the Lys-2 side chain residue, which in turn shift the electrostatic balance of the ion pair network and become hydrophobic (Fig. 7). Glycation of γB-crystallin at the N-terminus would lead to the removal of a positive charge, this alteration of surface charge would be likely to affect protein-protein and

protein-water interactions within the lens possibly perturbing short-range order and compromising the transparency of the lens (*Beswick and Harding, 1987*).

Corresponding author:
Dr. Alaa El-Din A. Abdel-Gawad,
Biophysics and Laser Science Unit, Research Institute of Ophthalmology, Al-Ahram Str 2, 12111 Giza, EGYPT.
Tel: (+202) 35718305;
E-mail: alaael_din3@hotmail.com

References

1. Yang S-J, Chen C-Y, Chang G-D, Wen H-C, Chen C-Y, *et al.* (2013). Activation of akt by advanced glycation end products (AGEs): Involvement of IGF-1 receptor and caveolin-1. PLoS ONE 8(3): e58100.
2. Karve TM and K. Cheema AK (2011). Small changes huge impact: the role of protein posttranslational modifications in cellular homeostasis and disease. J Amino Acids 2011: 207691
3. Baynes JW, Watkins NG, Fisher CI, Hull CJ, Patrick JS, Ahmed MU, Dunn JA and Thorpe SR (1989) The Amadori product on protein: structure and reactions. Prog. Clin. Biol. Res. 304, 43-67.
4. Yin D and Chen K (2005). The essential mechanisms of aging: Irreparable damage accumulation of biochemical side-reactions. Exp Geront 40: 455–465
5. Neves D. (2013). Advanced glycation end-products: a common pathway in diabetes and age-related erectile dysfunction. Free Radic Res. 47 Suppl 1: 49-69.
6. Swamy MS, Abraham EC (1987). Lens protein composition, glycation and high molecular weight aggregation in aging rats. Invest Ophthalmol Vis Sci 28: 1693-701.
7. Duhaiman AS (1995). Glycation of human lens proteins from diabetic and (nondiabetic) senile cataract patients. Glycoconj J 12: 618-21.
8. Jansirani and Anathanaryanan PH (2004). A comparative study of lens protein glycation in various forms ofcataract. Indian J Clin Biochem 19: 110-112.
9. Hollenbach S, Thampi P, Viswanathan T and Abraham EC (2003). Cleavage of *in vitro* and *in vivo* formed lens protein cross-links by a novel cross-link breaker. *Mol Cell Biochem* 243: 73–80.
10. Michael R and Bron AJ (2011). The ageing lens and cataract: a model of normal and pathological ageing. *Phil. Trans. R. Soc. B* 366: 1278–1292
11. Mega, T. L.; Cortes, S.; Van Etten, R. L (1990). The oxygen-18 isotope shift in carbon-13 nuclear magnetic resonance spectroscopy. 13. Oxygen exchange at the anomeric carbon of D-glucose, D-mannose, and D-fructose. J. Org. Chem. 55: 522–528.
12. Bell RC, Carlson JC, Storr KC, Herbert K,and Sivak J (2000). High-fructose feeding of streptozotocin-diabetic rats is associated with increased cataract formation and increased oxidative stress in the kidney. Br J Nutr 84: 575-582
13. Gul A, Rahman MA, Hasnain SN (2009). Role of fructose concentration on cataractogenesis in senile diabetic and non-diabetic patients. Graefe's Arch Clin and Exp Ophthalmol 247: 809-814
14. Sharma KK, Santhoshkumar P (2009). Lens aging: effects of crystallins. Biochim Biophys Acta 1790: 1095-108.
15. Mandal K, Chakrabarti B, Thomson J, Siezen RJ (1987). Structure and stability of gamma-crystallins. Denaturation and proteolysis behavior. J Biol Chem 262: 8096-102.
16. Casey EB, Zhao HR, Abraham EC (1995). Role of glycine 1 and lysine 2 in the glycation of bovine gamma B-crystallin. Site-directed mutagenesis of lysine to threonine. J Biol Chem. 270: 20781-6.
17. Alaa El-Din A. Gawad (2012). In silico docking analysis of rat γ-crystallin surfaces. JCoMod 2: 31-66.
18. Salim A, and Zaidi ZH. (2003). Homology models of human gamma-crystallins: structural study of the extensive charge network in gamma-crystallins. Biochem Biophys Res Commun 300: 624-30.
19. Zhen Xia, Zaixing Yang, Tien Huynh, Jonathan A. King & Ruhong Zhou (2013). UV-radiation induced disruption of dry-cavities in human γD-crystallin results in decreased stability and faster unfolding. *Scientific Reports* 3: 1560.
20. Alaa El-Din A. Gawad and Medhat A Ibrahim (2013). Computational studies of the interaction of chitosan nanoparticles and αB-crystallin. BioNanoSci 3: 302-311.
21. Lin, H., & Truhlar, D.G. (2005). Redistributed charge and dipole schemes for combined quantum mechanical and molecular mechanical calculations. *J Phys Chem A*, 109: 3991-4004.
22. Lodola A, Woods CJ and Mulholland AJ (2008). Applications and advances of QM/MM methods in computational enzymology. Ann Rep Comput Chem 4: 155-169.
23. Steinbrecher T, Elstner M (2013). QM and QM/MM simulations of proteins. Methods Mol Biol 924: 91-124
24. Mulholland AJ (2007). Chemical accuracy in QM/MM calculations on enzyme-catalysed reactions. Chem Cent J 1: 19.
25. Elstner M, Porezag D, Jungnickel G, Elsner J, Haugk M, Frauenheim Th, Suhai S, and Seifert G (1998). Self-consistent-charge density-functional tight-binding method for simulations of complex materials properties. Phys. Rev. B 58: 7260–7268.

26. Wickstrom L, Okur A, and Simmerling C (2009). Evaluating the performance of the ff99SB force field based on NMR scalar coupling data. Biophys J 97: 853–856
27. Kumaraswamy VS, Lindley PF, Slingsby C, and Glover ID (1996). An eye lens protein-water structure: 1.2 a resolution structure of gammaB-crystallin at 150 K. Acta Cryst D52: 611-622.
28. Garner WH, Balaji VN (1988). Structure analysis of bovine lens calf gamma-II crystallin: residue assignments of the five histidine CE1 resonances observed by proton-nuclear magnetic resonance spectroscopy. Curr Eye Res 7: 777-88.
29. Schüttelkopf AW, van Aalten DM (2004). PRODRG: a tool for high-throughput crystallography of protein-ligand complexes. Acta Crystallogr D Biol Crystallogr 60: 1355-63.
30. Vanquelef E, Simon S, Marquant G, Garcia E, Klimerak G, Delepine JC, Cieplak P, Dupradeau FY (2011). R.E.D. Server: a web service for deriving RESP and ESP charges and building force field libraries for new molecules and molecular fragments. Nucleic Acids Res: W511-7.
31. Gleeson MP, Burton NA, Hillier IH (2003). Prediction of the potency of inhibitors of adenosine deaminase by QM/MM calculations. Chem Commun (Camb). 7: 2180-1.
32. Salomon-Ferrer R, Case DA, Walker RC (2013). An overview of the Amber biomolecular simulation package. *WIREs Comput. Mol. Sci.* 3: 198-210.
33. Hornak V, Abel R, Okur A, Strockbine B, Roitberg A, and Simmerling C (2006). Comparison of multiple amber force fields and development of improved protein backbone parameters. PROTEINS: Structure, Function, and Bioinformatics 65:712–725
34. Mark P and Nilsson L (2001). Structure and Dynamics of the TIP3P, SPC, and SPC/E Water Models at 298 K. J. Phys. Chem. A 105: 9954-9960
35. Pastor RW, Brooks BR, and Szabo A (*1988*). An analysis of the accuracy of langevin and molecular-dynamics algorithms. Mol Phys 65:1409--1419
36. Ryckaert, J-P; Ciccotti G, Berendsen HJC (1977). "Numerical integration of the cartesian equations of motion of a system with constraints: molecular dynamics of *n*-alkanes". J Comput Phys 23: 327–341.
37. Berendsen HJC, Postma JPM, van Gunsteren WF, Di Nola A, and Haak JP (1984). Molecular dynamics with coupling to an external bath. J Chem Phys 81: 3684–3690.
38. Lin H, Truhlar DG (2005). Redistributed charge and dipole schemes for combined quantum mechanical and molecular mechanical calculations. J Phys Chem A 109: 3991–4004.
39. Darden T, York D and Pedersen L (1993). Particle mesh Ewald: An *N*·log(*N*) method for Ewald sums in large systems. J. Chem. Phys. **98**, 10089 (1993)
40. Humphrey W, Dalke A and Schulten K (1996). "VMD - Visual Molecular Dynamics". J. Molec. Graphics 14: 33-38.
41. Elstner M (2006). The SCC-DFTB method and its application to biological systems. Theor Chem Acc 116: 316-325.
42. Barnett CB,and Naidoo KJ (2010). Ring puckering: A metric for evaluating the accuracy of AM1, PM3, PM3CARB-1 and SCC-DFTB carbohydrate QM/MM simulations. *J Phys Chem B* 114: 17142–17154.
43. Mota JF, Blanco JLJ, Mellet CO, García Fernández JM (1994). 1-Doexy-1-isothiocyanato-D-fructose as intermediate in syntheses of 1,3-O(S),N-heterocycles. Carbohydrate Res 257: 127.
44. Cremer D, Pople JA (1975). General definition of ring puckering coordinates. J Am Chem Soc. 97: 1354–1358.
45. Johnson RJ, Sanchez-Lozada LG, Nakagawa T (2010). The effect of fructose on renal biology and disease. J Am Soc Nephrol. 2010 Dec;21(12):2036-9.
46. Franke S, Dawczynski J, Strobel J, Niwa T, Stahl P, Stein G (2003). Increased levels of advanced glycation end products in human cataractous lenses. J Cataract Refract Surg. 29: 998-1004.
47. Liang JN and Chakrabarti B (1981). Glycosylation-induced structural changes in bovine lens crystallins. Invest. Ophthalmol. *20* (Suppl.): 129
48. Beswick HT, Harding JJ (1987). Conformational changes induced in lens alpha- and gamma-crystallins by modification with glucose 6-phosphate: Implications for cataract. Biochem J 246: 761-769.
49. Imperiali B and O'Connor SE (1999). Effect of N-linked glycosylation on glycopeptide and glycoprotein structure. Curr. Opin. Chem. Biol. 3: 643–649.
50. Tams JW and Karen G. Welinder (2001). Kinetic stability of designed glycosylation mutants of coprinus cinereus peroxidase. Biochem Biophys Res Commun 286: 701–706.
51. Zhao H-R, Nagaraj RH and Abraham EC (1997). The Role of α- and ε-Amino Groups in the Glycation-mediated Cross-linking of γB-crystallin. Study of three site-directed mutants. J. Biol. Chem. 272: 14465-14469.